

## The Nature of Laves Phases

Guido Kreiner, Carsten Albrecht<sup>1</sup>, Rafik Ballou<sup>2</sup>, Ewald Bischoff<sup>3</sup>, Horst Borrmann, Manuel Brando, Wilder Carrillo-Cabrera, William Duncan<sup>1</sup>, Bjorn Fåk<sup>4</sup>, Malte Grosche<sup>1</sup>, Daniel Grüner<sup>5</sup>, Alexander Kerkau, Alim Ormeci, Yurii Prots, Walter Schnelle, Arndt Simon<sup>6</sup>, and Yuri Grin

### Introduction

The inter-institutional research initiative called “*The Nature of Laves Phases*” is a co-operation of four Max Planck institutes [1] with a strong interdisciplinary character. The Laves phases, which form the largest group of intermetallic compounds, are chosen as model systems for the experimental and theoretical investigations.

The research group for *Microstructure Physics* (D. Raabe, F. Stein, M. Palm) at the MPI für Eisenforschung GmbH in Düsseldorf puts its emphasis on understanding phase equilibria in binary and ternary systems and on the mechanical behavior of alloys. The project of the research field *Physical-Chemical Metallurgy* (E. J. Mittemeijer, A. Leineweber) at the MPI für Metallforschung, Stuttgart, is concerned with defect structures and phase transformations while the group for *Preparative Solid State Chemistry* (M. Jansen, D. Fischer) at the MPI für Festkörperforschung, Stuttgart, characterizes the crystallographic and electronic structure of metastable Laves phases. In Dresden at the MPI für Chemische Physik fester Stoffe, Laves phases are studied with respect to their formation, thermodynamic stability, chemical bonding and physical properties.

Here, we report exemplarily on three cooperations: (i) an investigation of the phenomenon of preferential site occupation of ternary Laves phases; (ii) the magnetic phase diagram of the Laves phase  $\text{Nb}_{1-y}\text{Fe}_{2+y}$ ; (iii) a study of chemical bonding. Details on the work, where Dresden has made contributions, are given in the following articles: site occupation reversal in the C14 Laves Phase  $\text{Nb}(\text{Cr}_{1-x}\text{Co}_x)_2$  [2,3]; the chemical bonding in Laves phases revised [4,5]; unusual mechanical behavior of the intermetallic phase  $\text{Nb}_2\text{Co}_7$  [6-9]; defect softening of  $\text{NbFe}_2$  and  $\text{NbCo}_2$  [10]; phase stability, structure and disorder of Co-Nb Laves phases [11-15]; ternary Laves phases [16-17]; the magnetic phase diagram of the Laves phase  $\text{Nb}_{1-y}\text{Fe}_{2+y}$  [18,19]; quantum critical phenomena in  $\text{NbFe}_2$  [18,20].

### Site occupation reversal in the C14 Laves phase $\text{Nb}(\text{Cr}_{1-x}\text{Co}_x)_2$

Many intermetallic compounds form broad compositional homogeneity ranges. Except for very simple crystal structures an element can occupy more than one crystallographic site. The distribution of the atoms of that element among different sites depends on temperature and composition. For a given composition one can distinguish three types of distribution: (i) random site occupation, (ii) ordered structures and (iii) preferential site occupation. The first case is characterized by the absence of short range order. In the second case there is short range order which is determined by the long range order of the crystal structure. In the third case the short range order is not determined by the long range order of the crystal structure, but depends on local interactions with a limited correlation length. To understand the phenomenon of preferential site occupation, it is essential to develop a proper description of phase stability.

An important example is ternary Laves phases of C14 structure type with the general formula  $A(B'_{1-x}B''_x)_2$ . Here, the usually smaller  $B$  atoms occupy the Wyckoff positions  $2a$  and  $6h$  of the space group  $P6_3/mmc$ . Experimental studies of ternary phase diagrams containing a C14 Laves phase along the section  $AB'_2-AB''_2$  have shown considerable homogeneity ranges for many systems. Thus far, only a few studies on C14  $A(B'_{1-x}B''_x)_2$  compounds dealt with the distribution of the  $B$  atoms among the two possible crystallographic positions. In case of  $\text{Ti}(\text{Fe}_{1-x}\text{Al}_x)_2$  [21] with  $0 \leq x \leq 0.165$  at 1000 °C, the Al atoms preferentially occupy the  $2a$  site. For  $\text{Zr}(\text{V}_{1-x}\text{Co}_x)_2$  [22] with  $0.2 \leq x \leq 0.7$  and  $\text{Ti}(\text{Mn}_{1-x}\text{Al}_x)_2$  [23] with  $0 \leq x \leq 0.67$  at 1000 °C the situation is more complex. Here, the respective minority component preferentially occupies the  $6h$  site. As an example in  $\text{Zr}(\text{V}_{1-x}\text{Co}_x)_2$ , at low Co content ( $x = 0.2$ ), the Co atoms prefer the  $6h$  site, whereas at high Co content ( $x = 0.7$ ) the  $6h$  site is favored by the V atoms. This phenomenon is known as site-occupation

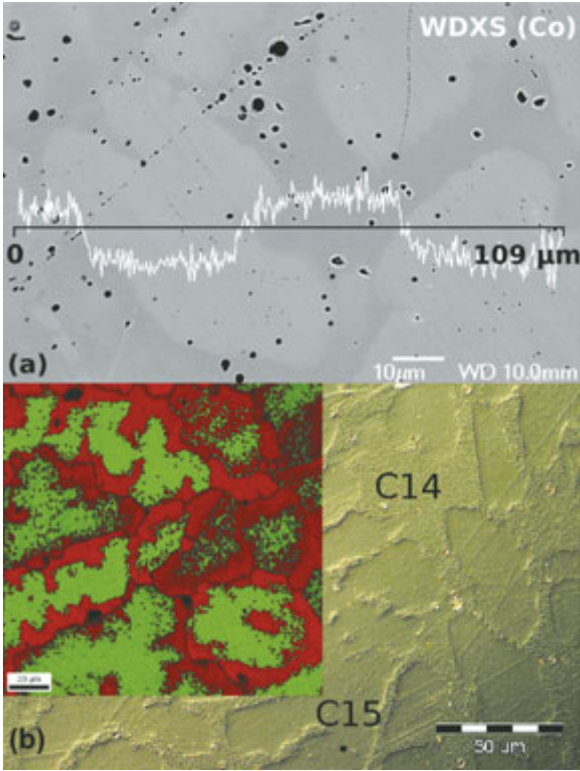


Fig. 1: (a) BSE image of a sample at the composition  $\text{Nb}_{33.3}\text{Cr}_{60.0}\text{Co}_{6.7}$ . WDXS line scan is overlaid. The Co-rich phase is C14. (b) Optical micrograph (DIC) of the same sample after etching. Rough surfaces correspond to the C14 phase. The inset shows an EBSD phase map. Red and green color indicate C14 and C15 Laves phases, respectively.

reversal and was first observed by Faller et al. [22] in the above mentioned C14  $\text{Zr}(\text{V}_{1-x}\text{Co}_x)_2$  phase. A series of Nb/Cr/Co alloys was prepared from high-purity starting materials by arc-melting and subsequent heat treatment at 1100 °C for 30 days. After annealing, the samples were quenched in water.

In order to study the site occupations in the C14 crystal structure of  $\text{Nb}(\text{Cr}_{1-x}\text{Co}_x)_2$  a statistical mechanical method based on first-principles total energy calculations is devised. In this approach the internal energy contributions are treated at a higher accuracy level, while the configurational phase space is much smaller in comparison to the more common Monte Carlo or molecular dynamics approaches.

The content of a unit cell of the  $\text{Nb}(\text{Cr}_{1-x}\text{Co}_x)_2$  Laves phase can be denoted as  $\text{Nb}_4\text{Cr}_{8-N}\text{Co}_N$ . For a given  $N$  between 2 and 6, we have considered all possible ways of distributing these  $N$  Co atoms over the  $2a$  and  $6h$  sites, assuming that the disordered crystal is represented by a canonical ensemble

of crystals each having one of the above configurations as its unit cell. Only Co concentrations of  $x = N/8$  can be studied by using this method. The idea is to compute the corresponding partition function  $Z_N$  for each  $N$ . Once  $Z_N$  is obtained, the thermal average of any physical quantity can be calculated by standard statistical mechanics rules. We performed first-principles total energy calculations only for those configurations that are symmetrically inequivalent. If there are  $M$  symmetrically inequivalent configurations each with multiplicity  $g$ , the partition function can be written in terms of these  $M$  different energy levels:

$$Z_N = \sum_{\sigma=1}^M g_{N,p;\sigma} \exp(-E_{N,p;\sigma} / (k_B T)).$$

Here,  $p$  denotes the number of Co atoms occupying the  $2a$  sites ( $p$  can be 0, 1 or 2) in a configuration indexed by  $\sigma$ .  $E_{N,p;\sigma}$  is the total energy of configuration  $\sigma$  computed by a first-principles scheme. The occupation of  $2a$  sites by Co atoms for a given  $N$  at a temperature  $T$  is then obtained from:

$$n_{\text{Co}}^{(2a)} = \frac{1}{Z_N} \sum_{\sigma=1}^M p \cdot g_{N,p;\sigma} \exp(-E_{N,p;\sigma} / (k_B T)).$$

For calculating  $n_{\text{Co}}^{(6h)}$ , replace  $p$  by  $(N-p)$  in the above expression.

The results as obtained from metallographic examinations, quantitative chemical analyses and X-ray powder diffraction studies show that the compound  $\text{Nb}(\text{Cr}_{1-x}\text{Co}_x)_2$  crystallizes with  $\text{MgZn}_2$  (C14) structure type with a broad homogeneity range of  $0.127(3) \leq x \leq 0.937(8)$  at 1100 °C. The width of the C14/C15 two-phase fields is about 2 at.% and 1 at.% for the Cr-rich and the Co-rich side, respectively. Due to the extremely small two-phase fields, the phases C14 and C15 cannot be distinguished unambiguously by usual optical microscopy but applying differential interference contrast (DIC) after etching (Fig. 1). A comparison with an EBSD phase map obtained from a polished surface of the same sample shows that the rough surfaces of the etched sample correspond to the C14 phase.

In experiment, both  $a$  and  $c$  lattice parameters of the hexagonal C14 unit cell decrease with increasing Co content, however, the  $c$  parameter with a steeper downward slope. The  $c/a$  ratio decreases with increasing Co content until a minimum is reached at the composition  $\text{Nb}(\text{Cr}_{0.2}\text{Co}_{0.8})$ . It then increases until the Co content is maximal at the

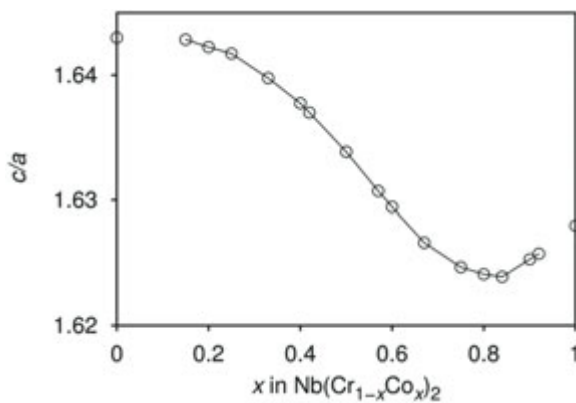


Fig. 2: Experimental determined axis ratio  $c/a$  for C14  $Nb(Cr_{1-x}Co_x)_2$  versus  $x$ . The values for C14  $NbCr_2$  and C14  $NbCo_2$  have been calculated by first-principle electronic structure calculations.

phase boundary (Fig. 2). The  $c/a$  ratio for the terminal phases C14  $NbCr_2$  and C14  $NbCo_2$  have been optimized by first-principles calculations because both phases are only stable as C15 structure type.

The results of the single crystal structure refinements for various compositions reveal substantial deviations from the idealized C14 crystal structure: (i) the networks of the smaller Cr or Co atoms and the Nb atoms are distorted; (ii) there is Cr/Co substitutional disorder at  $2a$  and  $6h$  Wyckoff sites with preferential occupation of the respective minority component at the  $2a$  site. The refinements clearly reveal a composition dependence of the site preference, including evidence for a site occupation reversal. In the case of the Cr-rich crystal ( $x = 0.33$ ), Co atoms prefer the  $M2$  ( $2a$ ) site, whereas in the Co-rich crystals ( $x = 0.67$  and  $0.80$ ), the  $M2$  ( $2a$ ) site is preferred by Cr atoms. In other words, the minority component prefers the  $2a$  site. The crystal with  $x = 0.50$  exhibits no preference of Cr/Co for either of the sites. The experimental results for the site occupation of Co at  $2a$  and  $6h$  sites are shown in Fig. 3a along with values obtained from the statistical mechanics approach. In addition, similar data for  $Zr(V_{1-x}Co_x)_2$  are shown in Fig. 3b with the experimental data taken from [22].

Although we only employed a simple statistical mechanical method, the computed values are seen to capture the observed trend, namely, composition-dependent site occupation reversal, for both systems. For  $Nb(Cr_{1-x}Co_x)_2$ , the  $6h$  Co occupation

is linearly dependent on Co concentration; the best line through the computed values coincides well with the line through the four experimental points. Regarding the  $2a$  occupation, computed values suggest that above some critical Co concentration (possibly somewhat higher than 50%), the occupation of the  $2a$  sites remains unchanged. However, experimental data do not show such saturation behaviour.

In the case of  $Zr(V_{1-x}Co_x)_2$ , the behaviour is much simpler. According to the available experimental data, the Co occupations of both the  $2a$  and  $6h$  sites follow straight lines. This development is well reproduced by the calculations, although the slopes of the curves slightly differ. Here, the calculations do not indicate a saturation of the  $2a$  occupation as found for  $Nb(Cr_{1-x}Co_x)_2$ .

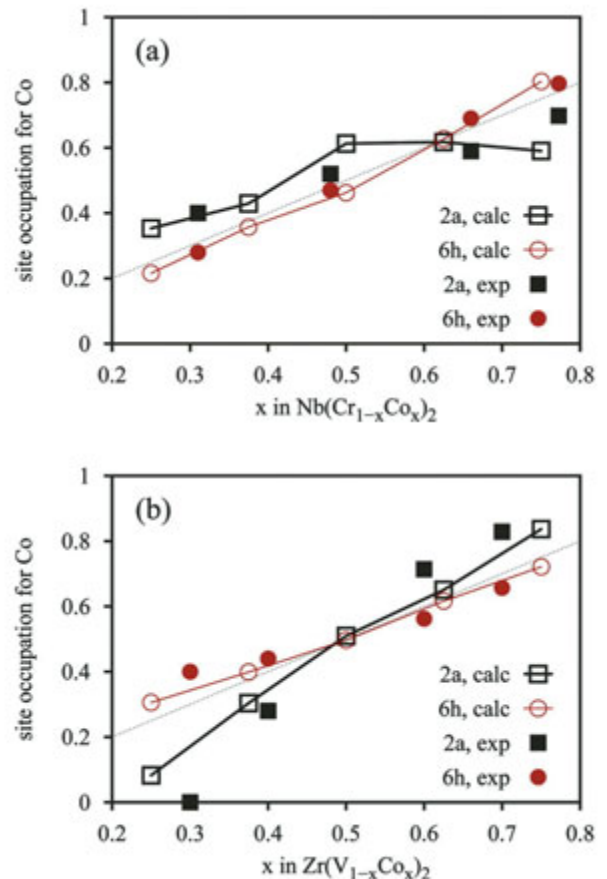


Fig. 3: Computed (open symbols) and experimental (filled symbols) Co occupations of the  $2a$  and  $6h$  site versus Co content  $x$  (a) for  $Nb(Cr_{1-x}Co_x)_2$  and (b) for  $Zr(V_{1-x}Co_x)_2$ . The dashed lines indicate a random distribution. Error bars smaller than size of symbols.

### Magnetic Phase Diagram of the C14 Laves Phase $\text{Nb}_{1-y}\text{Fe}_{2+y}$

The C14 Laves phase system  $\text{Nb}_{1-y}\text{Fe}_{2+y}$  exhibits three magnetically ordered low-temperature states within a narrow composition range at ambient pressure. At slightly off-stoichiometric compositions, both towards the iron-rich and the niobium-rich side, it has been reported to be ferromagnetic (FM), with composition-dependent, low transition temperatures  $T_C$  of the order of tens of Kelvin. At and very close to the stoichiometric composition,  $\text{NbFe}_2$  assumes antiferromagnetic or spin density wave (SDW) order below a second transition temperature  $T_N \sim 20$  K [24,25]. The easy accessibility of these ordered states in a nearly stoichiometric compound presents a number of interesting opportunities to study quantum phase transitions and quantum criticality in a transition metal compound [26].

Past studies of the  $\text{Nb}_{1-y}\text{Fe}_{2+y}$  system have explored the composition-temperature phase diagram in polycrystals by magnetic measurements and by nuclear magnetic resonance [24,25]. While in broad agreement, these studies differ in their classification of the slightly niobium-rich region of the phase diagram. The former (Ref. 24) describes the region around  $y \approx -0.01$  as paramagnetic down to 2 K, whereas the latter (Ref. 25) reports a mixed (FM and SDW) phase. Further microscopic probes have been Mössbauer spectroscopy, muon spin relaxation ( $\mu\text{sr}$ ) and neutron scattering studies. While  $\mu\text{sr}$  has shown evidence of static moments in stoichiometric  $\text{NbFe}_2$ , neutron scattering experiments have not revealed any information about the nature of this magnetic order in  $\text{NbFe}_2$  until now.

Here, we re-examine the magnetic phase diagram of  $\text{Nb}_{1-y}\text{Fe}_{2+y}$  in well-characterized high-quality samples. We aim to address key questions raised by earlier studies: (i) Does both FM phases previously observed, truly belong to the C14 phase of  $\text{Nb}_{1-y}\text{Fe}_{2+y}$  or is the ferromagnetism due to the presence of a FM second phase [27,28]; and (ii) does the antiferromagnetism disappear in slightly Nb-rich samples?

Since C14  $\text{Nb}_{1-y}\text{Fe}_{2+y}$  crystallizes in a broad homogeneity range from 27.4 to 36.3 at.% Nb at 1100 °C, and because the magnetic properties are very sensitive to  $y$ , it is important to verify not only the structure but also the final composition.

We therefore decided to prepare samples in the range of 26 to 40 at.% Nb, covering the whole homogeneity range of the C14 phase, accompanied by characterization with X-ray powder diffraction, metallographic analysis, and wavelength and energy dispersive X-ray spectroscopy (WDXS and EDXS). Pellets with a mass of 2 g were prepared by arc melting from pure niobium (H. C. Starck, granules, 99.9%) and iron (Chempur, foil, 99.997%) on a water-cooled copper hearth in an argon atmosphere. In order to assure homogeneity, the pellets were turned over and melted several times. The pellets were subsequently enclosed in weld-sealed niobium ampoules which were in turn jacketed in quartz tubes, and annealed at 1100 °C for three weeks. A phase of  $\text{Ti}_2\text{Ni}$  structure type is present in almost all investigated samples as impurity (see optical micrograph in Fig. 4). According to EDXS analysis this phase is richer in Nb compared to the Laves phase. Its probable composition is  $\text{Nb}_3\text{Fe}_2$ . The actual composition of this phase could not be accurately determined due to its small grain size. After having cut the samples into horizontal slices, we ground and polished them carefully and examined the surface with a high resolution optical microscope. The inset in Fig. 4 shows the optical micrograph taken from one of the upper slices. The  $\text{Nb}_3\text{Fe}_2$  phase can be clearly seen near the C14  $\text{NbFe}_2$  grain boundaries, its grains have dimensions of about 50  $\mu\text{m}$ . Afterwards, we measured the AC-magnetic susceptibility at low mag-

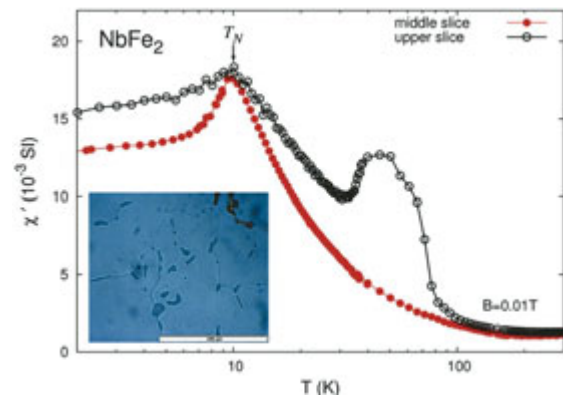


Fig. 4: AC-magnetic susceptibility of samples cut from the upper and middle slice of a pellet of a  $\text{NbFe}_2$  polycrystal. The measurements performed at low magnetic field (100 Oe) allow to detect the presence of FM phases at  $T_C \approx 80$  K in the upper slice sample in addition to the expected SDW peak ( $T_N \approx 10$  K). Comparing this measurement with the picture shown in the inset (the scale length is 100  $\mu\text{m}$ ), we deduce that the FM signal at  $T_C \approx 80$  K is caused by the second phase present around the  $\text{NbFe}_2$  grain boundaries.

netic fields ( $H \leq 250$  Oe) of samples extracted from the upper and the middle slice (Fig. 4): In the upper slice, we observed a FM signal with a transition temperature  $T_C \approx 80$  K, in addition to the expected SDW peak at  $T_N \approx 10$  K. In the middle slice, only the SDW signature is present. Comparing these measurements with the metallographic analysis, we conclude that the  $\text{Nb}_3\text{Fe}_2$  phase is responsible for the FM part of the signal.

The inset of Fig. 6 shows the average volume per atom of the C14 structure versus the nominal (solid line) and WDXS (dashed line) Nb content. In the range from 28 to 34 at.% Nb, a linear dependence of the atomic volume on composition determined by WDXS according to Vegard's volume rule is observed. Around the upper border of the homogeneity range the sample composition could not be determined accurately by WDXS, probably because of the large amount of the second phase. Using the relation

$$V_{\text{atom}} (\text{\AA}^3) = 12.0103 + 0.04024 \cdot x \text{ (at.\% Nb}_{\text{WDXS}})$$

we can determine the composition of a sample by measuring the unit cell parameters, which is especially useful to detect small differences in composition that are difficult to observe using WDXS. The estimated standard deviation of the WDXS measurements is of the order of 0.1 at.% limiting the accuracy on  $y$  to  $\sim 0.003$ . In addition, a small systematic error of about 0.2 at.% cannot be ruled out. However, the latter error shifts only the absolute value without changing the shape of the phase diagram (see below).

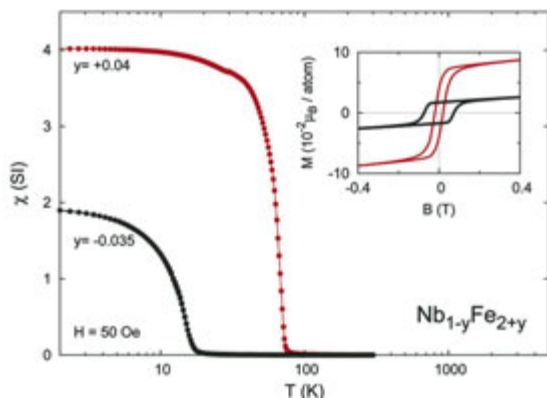


Fig. 5: Temperature dependence of the DC-magnetic susceptibility of  $\text{Nb}_{1-y}\text{Fe}_{2+y}$  samples with  $y = +0.04$  and  $y = -0.035$ . Inset: Hysteretic magnetization curves for the same samples. The Nb-rich sample shows a larger coercive field and smaller remanent magnetization.

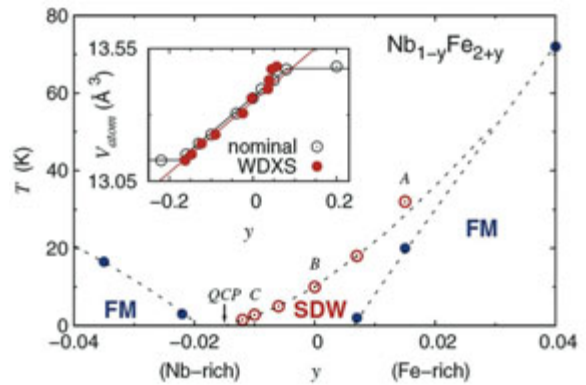


Fig. 6: Magnetic phase diagram: By adjusting the precise composition within a narrow homogeneity range,  $\text{NbFe}_2$  can be tuned from ferromagnetism (FM) ( $y > 0.01$ ) via an intermediate spin-density-wave (SDW) modulated state to a quantum critical point (QCP) ( $y \approx -0.015$ ). The precise composition has been determined from their unit cell parameters (from X-ray powder diffraction), which were compared against a scale drawn up by measuring the composition of a large number of samples covering the full homogeneity range using wavelength-dispersive X-ray spectroscopy (WDXS) (inset).

We focus our attention now on a very Nb-rich sample  $y = -0.035$ , as well as on one very rich in Fe with  $y = +0.04$ . They are still in the C14 homogeneity range and the amount of the  $\text{Nb}_3\text{Fe}_2$  phase appears to be negligible. Fig. 5 shows the DC magnetic susceptibility of the two samples measured at 50 Oe. Clear jumps in magnetization are observed at  $T \approx 72$  K and  $T \approx 14.5$  K for the Fe-rich and the Nb-rich sample respectively. When increasing the external field, the transition temperature remains practically constant, suggesting that the ferromagnetism is not a consequence of the second phase.

In addition, hysteresis signatures are evident in both samples, as shown in the inset of the same figure. Although in both samples the remanent magnetization is very small, in the order of  $10^{-2} \mu_B$  per atom, the coercive fields are quite large: 200 Oe and 700 Oe. Our results confirm that both Nb- and Fe-rich  $\text{Nb}_{1-y}\text{Fe}_{2+y}$  are FM with two different ferromagnetically ordered states [19].

We propose a refined version of the magnetic phase diagram for  $\text{Nb}_{1-y}\text{Fe}_{2+y}$  as stable at 1100 °C (Fig. 6), obtained by combining thermodynamic and transport measurements (not shown here) discussed in the references [18-20,29]. Dashed lines indicate the likely limits of the FM and SDW state. For  $|y| \geq 0.02$ , distinct FM phases have been observed at low temperature. Our data confirm that

the FM features do not originate from an impurity phase, but are intrinsic to the C14 Laves phase  $\text{Nb}_{1-y}\text{Fe}_{2+y}$ . A distinct non-FM phase has been observed between the FM phases: susceptibility, magnetization, resistivity and heat capacity results, many of which are similar to observations in well-known spin-helical compounds  $\text{MnAu}_2$  [30],  $\text{Y}_2\text{Fe}_{17}$  [31] and  $\text{MnSi}$ , suggest that the magnetic order assumes the form of a SDW, possibly a long wavelength helical or spiral state with an ordering wave vector of about  $0.05 \text{ \AA}^{-1}$  for  $\text{NbFe}_2$  [18]. On the Fe-rich side, we believe that the SDW state wave vector  $q \neq 0$  connects continuously to the FM state ( $q = 0$ ) at a point, which is located around  $y = +0.02$  [32]. Until the precise nature of the SDW state can be observed using a microscopic probe, ideally neutron scattering, this scenario remains strongly hypothetical. By reducing the Fe content (for small negative  $y$ ), the SDW state can be suppressed completely, leading to a magnetic quantum critical point (QCP) and leaving a small paramagnetic region around  $y \approx -0.015$ . Here, magnetic fluctuations dominate the temperature dependence of resistivity and specific heat. A detailed study of the quantum criticality in Nb-rich samples has been published elsewhere [18].

### Chemical bonding in Laves phases

Two rules, one geometric, other electronic, are discussed in regard to stability of Laves phases. The geometric rule gives sphere radii ratio of  $r_A/r_B = \sqrt{3/2} \sim 1.225$  as the most suitable one. The electronic rule suggests the valence electron concentration (electrons per atom) as responsible fac-

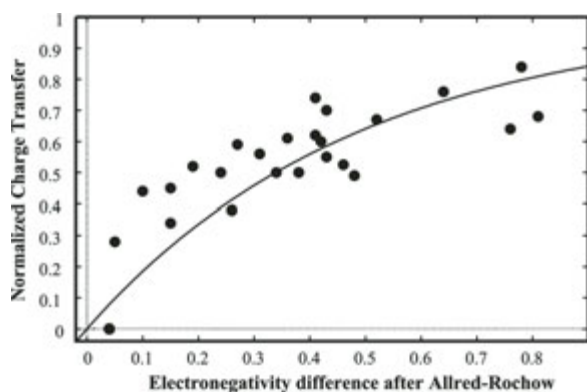


Fig. 7: QTAIM charge transfer vs electronegativity difference between the components A and B in selected Laves phases.

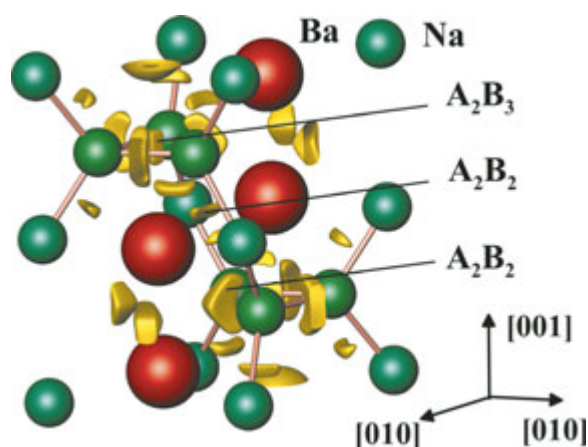


Fig. 8: Isosurface of ELI (yellow) in  $\text{BaNa}_2$  revealing the four- ( $A_2B_2$ ) and five-centre ( $A_2B_3$ ) bonding.

tor for formation of the main structural pattern of the Laves phases and its variation in different crystal-structure types. Recent analysis of the available information reveals that neither rule is obeyed [33], particularly, the radius ratio which varies between 1.05 and 1.70 for the known Laves phases. Already this finding alone suggests that chemical bonding effects may play an important role so that the tabulated values of atomic radii become effectively modified in the distinct compound as a result of chemical interactions and, thus, cannot be used directly as a parameter of a field for the description of the chemical bonding. The idea, as originally put forth in 1983 [34], is to investigate the compounds for which chemical bonding effects are expected to be minimal. Good candidates for this purpose are the Laves phases formed between the alkali metals. There are three known examples -  $\text{KNa}_2$ ,  $\text{CsNa}_2$  and  $\text{CsK}_2$ , all forming in the hexagonal C14 structure. As a first step towards a more comprehensive study, here we focus on the Cs-K system [4,5].

The two compounds existing in the K-Cs system, the C14 Laves phase  $\text{CsK}_2$  and the hexagonal  $\text{Cs}_6\text{K}_7$ , are studied by first-principles electronic structure calculations. Atom volumina and charge transfer analyses carried out within the framework of the quantum theory of atoms in molecules (QTAIM) suggest that already in alkali-metal-only compounds, where there is only one valence electron per atom, chemical bonding effects should be taken into account, and that the formation of the Laves phases  $\text{KNa}_2$ ,  $\text{CsNa}_2$  and  $\text{CsK}_2$  may not be explained on grounds of purely geometrical factors.

Stability of the structural patterns of Laves phases suggests a common driving force to realize the closest packing motif with different chemical elements. In order to evaluate the role of the charge transfer as a possible driving force, we investigated the atomic charges by means of the QTAIM in several Laves phases of the main group elements and transition metals.

The analysis of the relation between the normalized charge transfer and the electronegativity difference (Fig. 7) shows that, despite a relatively strong scattering of the data, the expected but not obvious general trend of charge transfer increases with the increasing electronegativity difference between A and B components. The best fits were obtained for the Sanderson's and Allred's electronegativities provided the zero charge transfer occurs for zero electronegativity difference, and maximal charge transfer is limited to unity at the maximal electronegativity difference. The trend observed indicate that the charge transfer contributes to the stabilization of the structural pattern of the most Laves phases investigated here beside BaNa<sub>2</sub>. In this compound the stabilizing role is obviously played by the multi-centre non-polar covalent bonding, as it was shown by applying the electron localizability indicator (see Scientific Report *New Developments in Electron Localizability*, ELI, Fig. 8).

## References

- [1] *The Nature of Laves Phases*, <http://laves.mpie.de>.
- [2] A. Kerkau, Diplomarbeit TU Dresden 2007.
- [3] A. Kerkau, D. Grüner, A. Ormeci, Yu. Prots, H. Borrmann, W. Schnelle, E. Bischoff, Yu. Grin, and G. Kreiner, *Z. Anorg. Chem.*, in press.
- [4] Yu. Grin, A. Simon, and A. Ormeci, *Mater. Res. Soc. Symp. Proc.*, (2008) in press.
- [5] A. Simon, A. Ormeci, Yu. Grin, Max-Planck-Institut für Festkörperforschung, Stuttgart, Annual Report 2007, p. 39-41.
- [6] F. Stein, M. Palm, G. Frommeyer, L. Siggelkow, D. Grüner, G. Kreiner, M. Mihalkovic, and A. Leineweber, *Mater. Res. Soc. Symp. Proc.*, in press.
- [7] L. Siggelkow, Diplomarbeit TU Dresden 2007.
- [8] L. Siggelkow, U. Burkhardt, G. Kreiner, M. Palm, and F. Stein, *Mater. Sci. Eng. A* **497** (2008) 174.
- [9] G. Frommeyer, Max-Planck-Institut für Eisenforschung GmbH, Düsseldorf, Scientific Report 2007/2008, p. 95-104.
- [10] S. Voss, F. Stein, M. Palm, D. Grüner, G. Kreiner, G. Frommeyer, and D. Raabe, *Mater. Res. Soc. Symp. Proc.*, (2008) in press.
- [11] D. Grüner, Dissertation, TU Dresden 2007.
- [12] G. Kreiner, D. Grüner, Yu. Grin, F. Stein, M. Palm, and A. Ormeci, *Mater. Res. Soc. Proc.*, (2008) in press.
- [13] F. Stein, D. Jiang, M. Palm, G. Sauthoff, D. Grüner, and G. Kreiner, *Intermetallics* **16** (2008) 785-792.
- [14] D. Grüner, F. Stein, M. Palm, J. Konrad, A. Ormeci, W. Schnelle, Yu. Grin, and G. Kreiner, *Z. Kristallogr.* **221** (2006) 319-333.
- [15] T. Yokosawa, K. Söderberg, M. Boström, D. Grüner, G. Kreiner, and O. Terasaki, *Z. Kristallogr.* **221** (2006) 357-374.
- [16] D. Grüner, A. Ormeci, and G. Kreiner, *Z. Kristallogr. - New Cryst. Struct.* **221** (2006) 3.
- [17] O. Prymak, F. Stein, A. Kerkau, A. Ormeci, G. Kreiner, G. Frommeyer, and D. Raabe, *Mater. Res. Soc. Symp. Proc.*, (2008) in press.
- [18] M. Brando, W. J. Duncan, D. Moroni-Klementowicz, C. Albrecht, D. Grüner, R. Ballou, and F.M. Grosche, *Phys. Rev. Lett.* **101** (2008) 026401.
- [19] D. Moroni-Klementowicz, M. Brando, C. Albrecht, W. J. Duncan, F. M. Grosche, D. Grüner, and G. Kreiner, *Phys. Rev. B*, submitted.
- [20] M. Brando, D. Moroni-Klementowicz, C. Albrecht, W. J. Duncan, D. Grüner, R. Ballou, B. Fåk, and F. M. Grosche, *J. Magn. Magn. Mater.* **310** (2007) 852.
- [21] X. Yan, X.-Q. Chen, A. Gritsiv, V.T. Witusiewicz, P. Rogl, R. Podlucky, V. Pomjakushin, G. Giester, *Inter. J. Mater. Res.* **97** (2006) 450-460.
- [22] J. G. Faller and L. P. Skolnick, *Transition Met. Soc. AIME*, **227** (1963) 687-695.
- [23] X. Yan, X.-Q. Chen, A. Gritsiv, P. Rogl, R. Podlucky, H. Schmidt, G. Giester, and X.-Y. Ding., *Intermetallics* **16** (2008) 16-26.
- [24] Y. Yamada and A. Sakata, *J. Phys. Soc. Jpn.* **57**, (1988) 46.
- [25] M. R. Crook and R. Cywinski, *J. Magn. Magn. Mater.* **140-144**, (1995) 71.
- [26] P. Gegenwart, Q. Si, and F. Steglich, *Nature Physics* **4**, (2008) 186.
- [27] Y. J. Bi, J. S. Abell, and D. Fort, *J. Crystal Growth* **166**, (1996) 298.
- [28] J. H. Zhu, L. M. Pike, C. T. Liu, and P. K. Liaw, *Acta mater.* **47** (1999) 2003.
- [29] M. Brando, D. Moroni-Klementowicz, C. Albrecht, and F. M. Grosche, *Physica B* **378-380** (2006) 111.
- [30] H. Samata, N. Sekiguchi, A. Sawabe, Y. Nagata, T. Uchida, and M. Der Lan, *J. Phys. Chem. Solids* **59** (1998) 377.
- [31] O. Prokhnenko, J. Kamarád, K. Prokeš, Z. Arnold, and A. V. Andreev, *Phys. Rev. Lett.* **94** (2005) 107201.
- [32] R. M. Hornreich, M. Luban, and S. Shtrikman, *Phys. Rev. Lett.* **35** (1975) 1678.
- [33] F. Stein, M. Palm, G. Sauthoff, *Intermetallics* **12** (2004) 713.
- [34] A. Simon, *Angew. Chem.* **95** (1983) 94.

---

<sup>1</sup> Department of Physics, Royal Holloway, University of London, Egham TW20 0EX, United Kingdom

<sup>2</sup> Institut Néel, CNRS and Université Joseph Fourier, BP 166, F-38042 Grenoble Cedex 9, France

<sup>3</sup> Max-Planck-Institut für Metallforschung, Stuttgart, Germany

<sup>4</sup> Commissariat à l'Énergie Atomique, Département de Recherche Fondamentale sur la Matière Condensée, SPSMS, 38054 Grenoble, France

<sup>5</sup> Present address: Department of Physical, Inorganic and Structural Chemistry, Arrhenius Laboratory, Stockholm University, Stockholm, Sweden

<sup>6</sup> Max-Planck-Institut für Festkörperforschung, Stuttgart, Germany